

Room-Temperature Indentation Creep and the Mechanical Properties of Rapidly Solidified Sn-Sb-Pb-Cu Alloys

Mustafa Kamal, A. El-Bediwi, A.R. Lashin, and A.H. El-Zarka

(Submitted December 23, 2014; in revised form January 7, 2016; published online March 31, 2016)

In this paper, we study the room-temperature indentation creep and the mechanical properties of Sn-Sb-Pb-Cu alloys. Rapid solidification from melt using the melt-spinning technique is applied to prepare all the alloys. The experimental results show that the magnitude of the creep displacement increases with the increase in both time and applied load, and the stress exponent increases with the increase in the copper content in the alloys which happens primarily due to the existence of the intermetallic compounds SbSn and Cu₆Sn₅. The calculated values of the stress exponent are in the range of 2.82 to 5.16, which are in good agreement with the values reported for the Sn-Sb-Pb-Cu alloys. We have also studied and analyzed the structure, elastic modulus, and internal friction of the Sn-Sb-Pb-Cu alloys.

Keywords hardness, indentation creep, rapid solidification, x-ray diffraction

1. Introduction

A fast, simple, and non-destructive method of investigating the mechanical properties of solid materials is called indentation creep test (Ref 1-9). The indentation creep tests have several advantages compared with the conventional creep experiments (Ref 1), e.g., in these tests small amounts of materials are needed and the method of preparing the sample is simple because only flat sample surface is required. Moreover, for example, the characterization of the local deformation behavior of thin films or particles in composites can be performed by indentation creep tests. In the Vickers hardness tests with a pyramid indenter or a cylindrical indenter, the net section stress under the indenter is constant in a constant load test, which is an advantage over other indentation techniques, whereas in other indenter geometries, the net section stress decreases with time (Ref 10-13). The indentation process demonstrates that a hard indenter maintains a constant load over a period of time and the changes in the size of the indentation are monitored as the indenter moves into the test specimen (Ref 1, 3, 8). The size of the indentation observed during the creep test depends on the quality of the material to deform plastically. The hardness test has been used effectively for studying the bulk deformation behavior, although the indenter is only in contact with the surface of the sample (Ref 4). The indentation creep process is characterized by the stress exponent n that is equal to the creep exponent of the material. The stress exponent can be used as an indicator of the creep mechanism (Ref

13, 14). It has been found that when the value of n is 1, creep is controlled by vacancy diffusion as deformation mechanism (Ref 14-16); when n is 2, the creep mechanism is controlled by grain boundary sliding (Ref 17); when n is 3, diffusion-controlled dislocation motion acts as deformation mechanism (Ref 17); when n is 4 to 7, it is attributed to dislocation climb-controlled creep mechanism (Ref 18); and when n is more than 8, creep is controlled by the reinforcement of particles (Ref 19).

Lead- and tin-based alloys are generally the first choice for developing materials that offer superior compatibility with steel shafts, their ability (due to their softness) to embed foreign particles and their unique ability to adapt to misalignment. Despite their higher cost, tin Babbitt are often preferred over lead Babbitt because of their excellent corrosion resistance, easy bonding, and less tendency toward segregation (Ref 20-25). Tin-based Babbitt alloys generally contain antimony and copper that have adequate hardness number, which provides excellent load-carrying characteristic (Ref 23, 24). In the absence of adequate lubrication, they also exhibit low friction resistance, low wear, good run-in properties, and good emergency behavior. In this paper, the room-temperature indentation creep and the mechanical properties of Sn-11%Sb-(9 - X)Pb-X%Cu alloys, where $X = 0, 1, 3,$ and 5 wt.%, have been studied.

2. Materials and Methods

In the present work, Sn-11%Sb-(9 - X)Pb-X%Cu alloys, where $X = 0, 1, 3,$ and 5 wt.%, were used as samples, and were melted in a muffle furnace using tin, antimony, lead, and copper with purity more than 99.5%. In order to increase the homogeneity, the resulting ingots were turned and re-melted four times. These ingots were rapidly solidified from melt. The rapid solidification was achieved by a single copper roller type melt-spinning technique. The surface velocity of the roller was 31.4 m/s corresponding to 3.7×10^5 K/s (Ref 26). All samples were quenched in air. The samples were then divided into convenient shapes for the measurements using double knife

Mustafa Kamal, A. El-Bediwi, and A.H. El-Zarka, Metal Physics Lab, Physics Department, Faculty of Science, Mansoura University, Mansoura 35516, Egypt; and **A.R. Lashin**, Metal Physics Lab, Physics Department, Faculty of Science, Mansoura University, Mansoura 35516, Egypt; and Physics Department, Faculty of Applied Science, Umm Al-Qura University, Mecca 21955, Saudi Arabia. Contact e-mail: lashingi@mans.edu.eg.

cutter. Typical dimensions of samples (ribbons) were about 5 mm in width, 60 μm in thickness, and 5 cm in length.

The dynamic resonance method was used to determine the internal friction, Q^{-1} , and the elastic constants. The value of the dynamic Young modulus E is determined by the following equation (Ref 27-29):

$$\left(\frac{E}{\rho}\right)^{1/2} = \frac{2\pi L^2 f_0}{kz^2}, \quad (\text{Eq 1})$$

where ρ is the density of the sample used in the test, L is the length of the vibrated part of the sample, k is the radius of gyration of the cross-section perpendicular to its plane of motion, f_0 is the resonance frequency, and z is a constant which depends on the mode of vibration and is equal to 1.8751. The resonance curve is drawn by plotting the amplitude of vibration against the frequency of vibration around the resonance f_0 . The internal friction, Q^{-1} , of the sample can be determined by the following equation:

$$Q^{-1} = 0.5773 \frac{\Delta f}{f_0}, \quad (\text{Eq 2})$$

where Δf is the half-width of the resonance curve.

A Shimadzu x-ray diffractometer (DX-30) using Cu $K\alpha$ radiation with a Ni filter ($\lambda = 1.5406 \text{ \AA}$) was used to carry out x-ray diffraction analysis (XRD). The microstructure was examined with a Joel SEM (Joel Corp., Mikaka, Japan). The Vickers microhardness tester (Model-FM7-Japan) with loads of 10, 25, and 50 g force (gf) for dwell times 5 up to 90 s was applied to study the creep indentation behavior of the used samples. Each reading was an average of at least six separate measurements taken at random places in both x - and y -directions on the surface of the sample. The readings had an accuracy of 0.01 μm . All the indentations were at a distance of minimum 0.5 mm from the edges and other indentations.

3. Results and Discussion

3.1 X-ray Diffraction Measurements

The XRD diffraction patterns of rapidly solidified alloys that were converted from melt Sn-11%Sb-(9 - X)%Pb-X%Cu alloys (where X = 0, 1, and 3 wt.%) show the corresponding lines of β -Sn, α -Pb, and SbSn phases as shown in Fig. 1(a) to

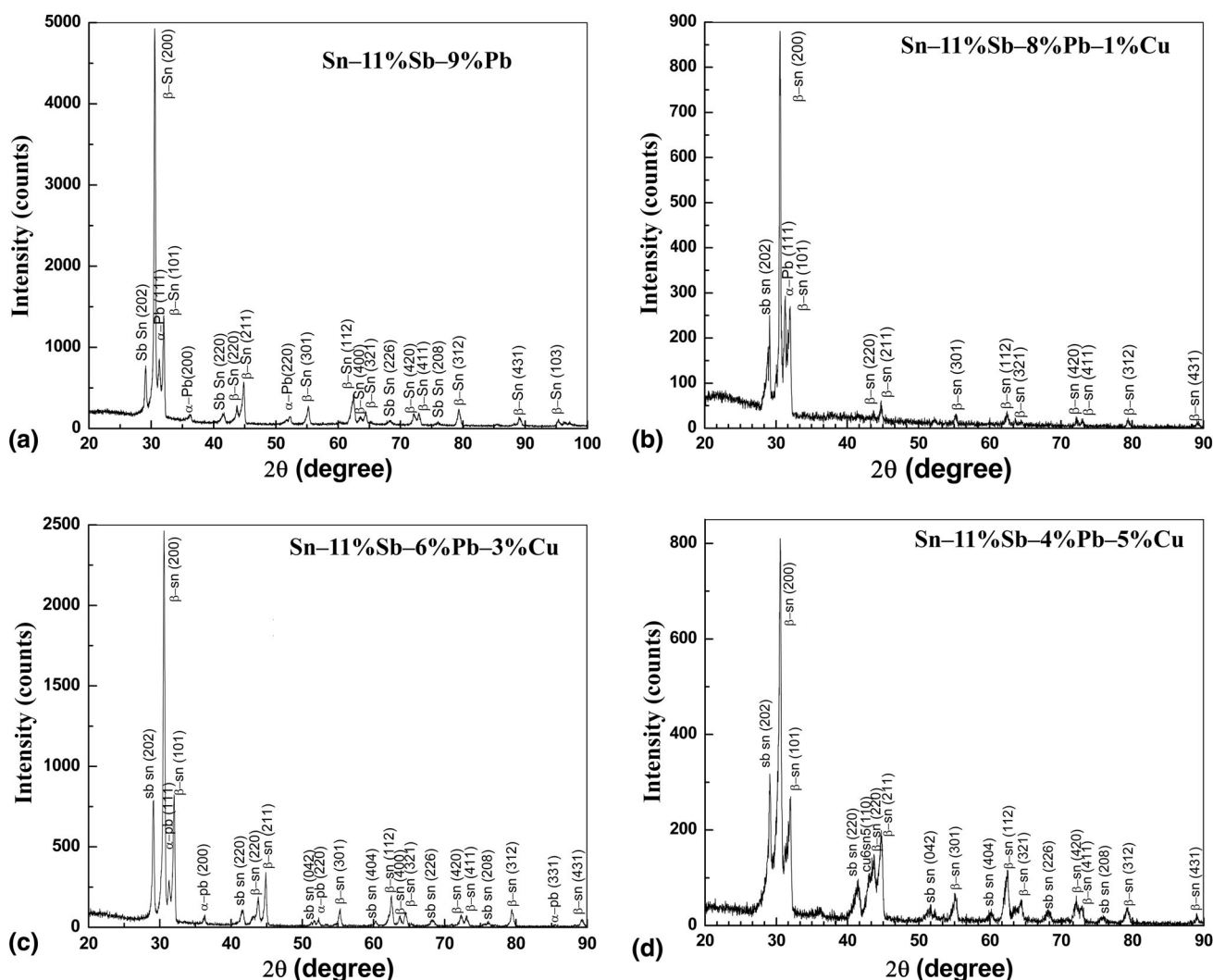


Fig. 1 X-ray diffraction patterns of the Sn-11%Sb-9%Pb (a), Sn-11%Sb-8%Pb-1%Cu (b), Sn-11%Sb-6%Pb-3%Cu (c), and Sn-11%Sb-4%Pb-5%Cu (d) alloys

Table 1 Stress exponent, Young's modulus, internal friction, and lattice particle size of the Sn-11%Sb-(9 - X)%Pb-X%Cu alloys, where X = 0, 1, 3, and 5 wt.%

Alloy	The average Stress exponent	Young's Modulus, GPa	The internal friction, Q ⁻¹	The average lattice size, Å
Sn-11%Sb-9%Pb	2.82 ± 0.17	14.8 ± 0.48	0.0352 ± 0.0023	405.86 ± 2.35
Sn-11%Sb-8%Pb-1%Cu	3.18 ± 0.17	16.9 ± 2.19	0.0351 ± 0.0014	355.45 ± 4.57
Sn-11%Sb-6%Pb-3%Cu	3.57 ± 0.14	18.6 ± 1.22	0.0329 ± 0.0013	335.22 ± 3.60
Sn-11%Sb-4%Pb-5%Cu	5.16 ± 0.17	20.2 ± 3.10	0.0355 ± 0.0019	229.41 ± 1.78

(c). In addition to the lines corresponding to β-Sn, α-Pb, and SbSn phases, extra lines of Cu₆Sn₅ intermetallic compounds were found for rapidly quenched alloys that contain 5 wt.% Cu (Fig. 1(d)).

The Scherrer method is used to calculate the crystal sizes obtained from the X-ray patterns (Ref 30, 31). According to this method, if the crystallites that are used to prepare a powder specimen are sufficiently small, the maxima of the diffraction pattern are increased by an amount inversely proportional to the crystallite size, and the crystal size is given by the following equation:

$$y = a \frac{\lambda}{b \cos \theta}, \quad (\text{Eq 3})$$

where y is the crystal size, λ is the wavelength of the radiation, b is the additional broadening (in radians), θ is the Bragg's angle, and a is a dimensionless number of the order of unity (≈ 0.9 for the alloys used in this paper), which is known as the Scherrer constant. Table 1 shows the average crystal sizes of different phases for the Sn-11%Sb-(9 - X)%Pb-X%Cu alloys (where X = 0, 1, 3, and 5 wt.%).

As the average crystal size of the β-Sn matrix is greater than that of the intermetallic compounds (SbSn and Cu₆Sn₅) (Ref 32), as shown in Table 1, it is shown that the average crystal size decreases with the increase in the concentration of copper at the expense of lead. The presence of these intermetallic compounds with small crystal sizes implies that the alloys are melted using the grain-refining process. The fine-grained materials are harder and stronger than those that are produced using coarse-grained materials, since the former have a greater total grain boundary area to impede the dislocation motion. Note that the reduction in the size of the grain not only improves the strength, but also enhances the ductility and the toughness of these alloys (Ref 33). Although Cu was not detected in the alloys containing 1 and 3 wt.% copper, its effect is clearly appeared in mechanical properties of these alloys as shown in Table 1. Rapid solidification with high cooling rate increases the Cu solubility (Ref 34, 35); therefore, copper was dissolute to form a solid solution with the matrix.

3.2 Microstructural Examination

Figure 2(a) and (b) displays the scanning electron microscope images of the Sn-11%Sb-8%Pb-1%Cu and Sn-11%Sb-4%Pb-5%Cu alloys, respectively. The morphology of the surface is different in both alloys. Figure 2(a) contains Sn-rich phase (matrix) with some precipitates of SbSn and Pb phases. The intermetallic compound Cu₆Sn₅ has been appeared in the microstructure of the Sn-11%Sb-4%Pb-5%Cu alloy. However, it is clear that the particle size in Sn-11%Sb-4%Pb-5%Cu is finer than that in the Sn-11%Sb-8%Pb-1%Cu alloy. This is in agreement with the crystal size measurements that are obtained by the x-ray diffraction (Table 1).

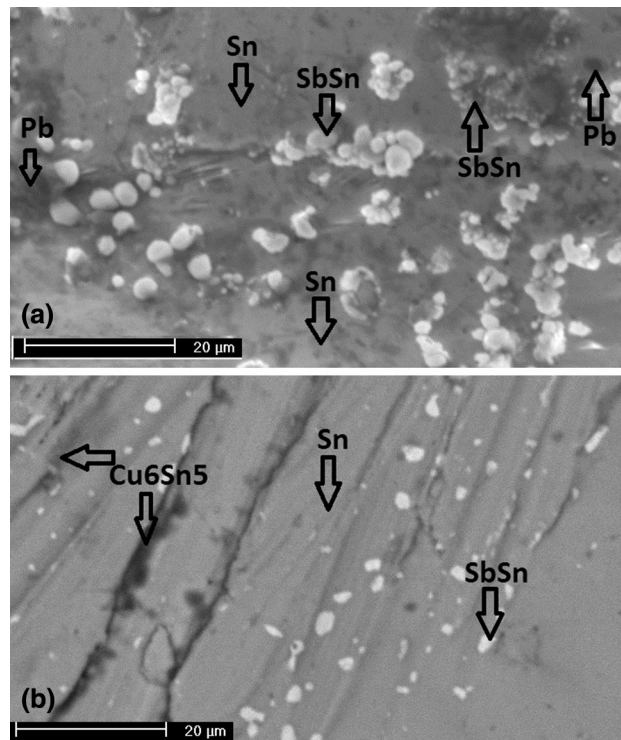


Fig. 2 Scanning electron microscope (SEM) images for the Sn-11%Sb-8%Pb-1%Cu alloy (a) and the Sn-11%Sb-4%Pb-5%Cu alloy (b)

3.3 Indentation Creep Measurements

The normal creep curve consists three stages: (1) transient creep that starts at a fairly rapid rate which then decreases with time as strain hardening sets in, (2) steady-state creep in which the rate of strain is fairly uniform and at its lowest value and (3) tertiary creep in which the rate of strain increases rapidly so that fracture occurs (Ref 36). In the indentation creep, the shape of the indentation curve is the same as that of an ordinary creep curve. The only difference is that in the indentation creep the last stage does not appear. This happens because the hardness test is actually a compression test, the fracture of the specimen does not occur and hence it is obviously not possible to measure a third stage of the curve (Ref 37).

Generally, the steady-state stress exponent, n , is used to describe the variation in the steady-state creep rate with the applied stress which is given by the following equation (Ref 38):

$$n = \left[\frac{\partial \ln \dot{\epsilon}}{\partial \ln \sigma} \right]_T, \quad (\text{Eq 4})$$

where $\dot{\epsilon}$ the strain rate and σ is the tensile stress at a constant temperature T . An analogy relationship described by Juhasz et al. used to analyze the indentation creep (Ref 39) which can be shown in the following form:

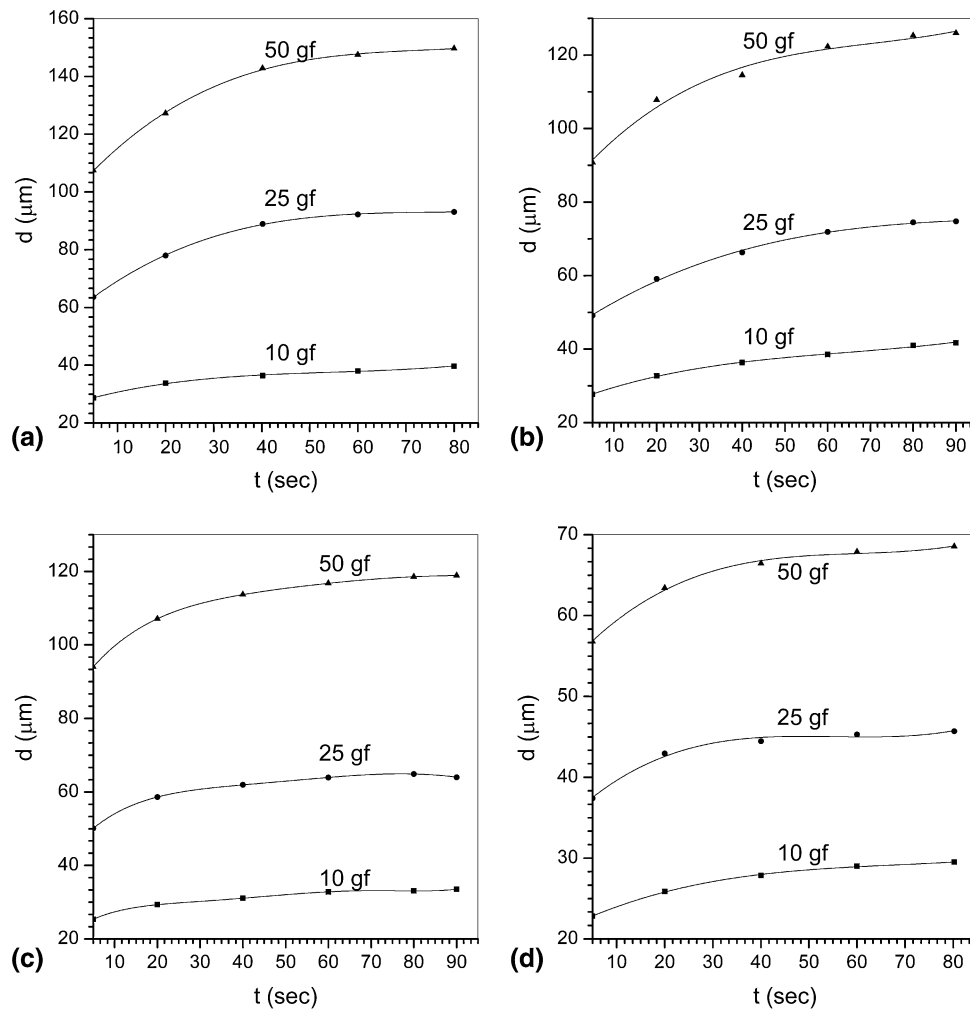


Fig. 3 Indentation displacement, d , vs. indentation time, t , of the: Sn-11%Sb-9%Pb (a), Sn-11%Sb-8%Pb-1%Cu (b), Sn-11%Sb-6%Pb-3%Cu (c), and Sn-11%Sb-4%Pb-5%Cu (d) alloys at load 10, 25, and 50 g force

$$n = \left[\frac{\partial \ln \dot{d}}{\partial \ln H_v} \right]_d, \quad (\text{Eq } 5)$$

where $H_v = C(F/d^2)$ is the Vickers hardness number, \dot{d} is the rate of variation in indentation length, d is the indentation diagonal length, C is a constant, and F is the applied load. This implies that a straight line would be obtained, the slope of which is the stress exponent n , if \dot{d} is plotted against H_v on a double logarithmic scale.

For the Sn-11%Sb-(9 - X)Pb- X %Cu alloys, where $X = 0, 1, 3,$ and 5 wt.%, the indentation length is plotted against time at different constant loads 10, 25, and 50 gf as shown in Fig. 3(a) to (d). This figure indicates that the indentation length increases with the loading time and the applied load. Figure 4(a) to (d) displays the logarithm of the rate of variation of indentation displacement against the logarithm of the Vickers hardness number of the Sn-11%Sb-(9 - X)Pb- X %Cu alloys, where $X = 0, 1, 3,$ and 5 wt.% at loads 10, 25, and 50 gf according to Eq 5. Table 1 shows the values of stress exponents that are obtained. The values of stress exponents obtained from indentation curves range between 2.82 and 5.16. It is also found that by increasing the concentration of copper at the

expense of lead, the stress exponent increases, which indicates that room-temperature creep takes place less rapidly.

The change in stress exponent values is attributable to microstructural change in the matrix, such as change in the lattice parameters, solid solution, size and distribution of strengthening phases, intermetallic phases (Ref 24). Decreasing the grain size by increasing the Cu content increases the grain boundaries that act as more effective barriers to dislocation movement and hence the stress exponent values increase as shown in Table 1.

3.4 Young's Modulus and Internal Friction Measurements

One of the important characteristics that strongly reflect the interaction and the bonding nature of the constituent atoms is known as Young's modulus (Ref 40). The magnitude of the elastic constant of defect-free metal alloys is merely a function of the magnitude of the stiffness of the atomic bonds. Other factors such as porosity, concentration of impurities, intergranular phases, and alloying elements may influence the magnitude of the elastic constants in real polycrystalline melt-spun alloys. The nominal elastic modulus value of Sn and its alloys is generally considered as 50 GPa, but the experimental values of

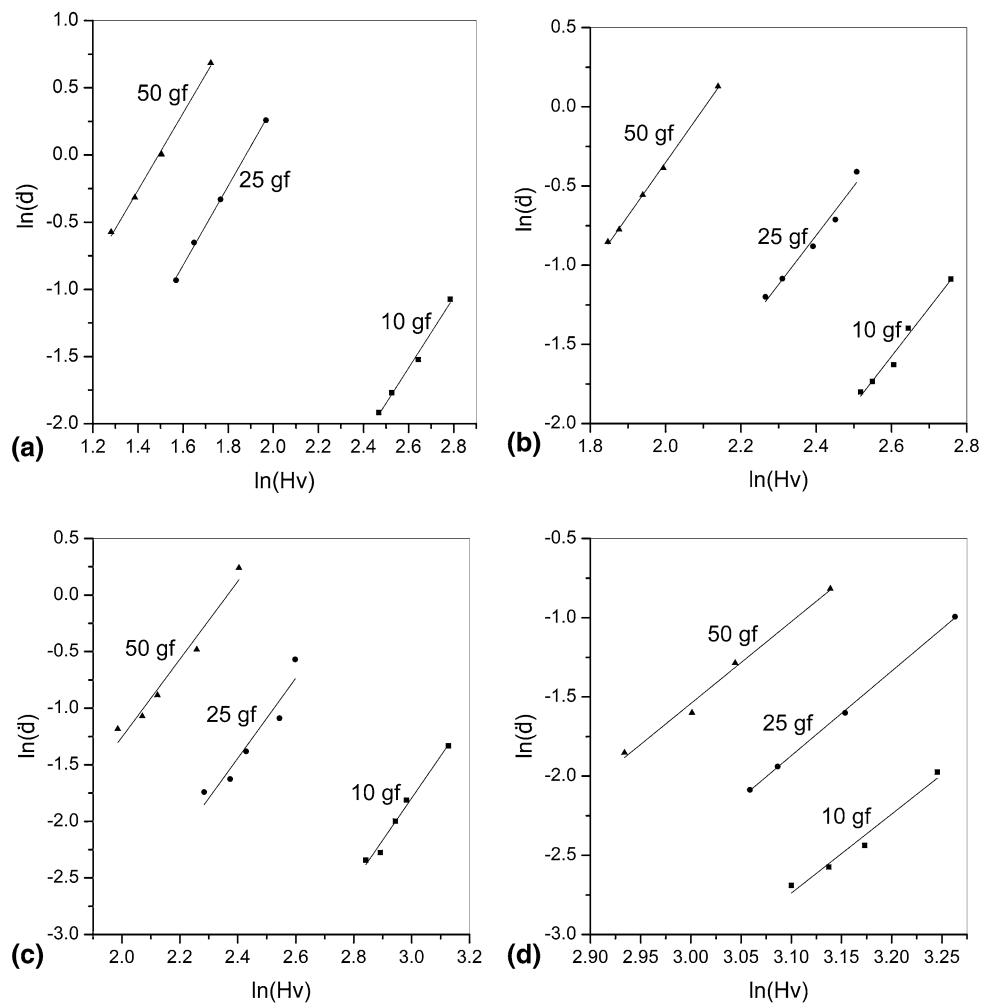


Fig. 4 The logarithm of the rate of variation of indentation displacement vs. the logarithm of Vickers hardness number of the: Sn-11%Sb-9%Pb (a), Sn-11%Sb-8%Pb-1%Cu (b), Sn-11%Sb-6%Pb-3%Cu (c), and Sn-11%Sb-4%Pb-5%Cu (d) alloys at load 10, 25, and 50 g force

pure tin and its alloys can vary between 16 and 55 GPa as reported from the literature (Ref 41). The resonance curves of melt-spun alloys Sn-11%Sb-(9 - X)%Pb-X%Cu, where X = 0, 1, 3, and 5% Cu, are shown in Fig. 5. The calculated values of the elastic modulus of each alloy are listed in Table 1. Note that the value of the elastic modulus increases with the increase in the concentration of Cu at the expense of lead. The bonding force among atoms is used to determine Young's modulus. Therefore, the bonding force is not only related to the crystal structure, but also to the distance among atoms and it can be affected by alloying additions (Ref 42). In addition, it is observed that Cu atoms tend to interact much more strongly with Sn than Sb and Pb to form high melting point intermetallic compound Cu_6Sn_5 as compared with $SbSn$ compound (Ref 43). Therefore, for melting an alloy, a small amount of copper is added to facilitate the formation of yet another metallic compound Cu_6Sn_5 and to increase the elastic modulus of the Sn-Pb-Sb melt-spun bearing alloy. Usually, two common intermetallic compounds are obtained from the interaction of Cu with the liquid Sn, they are Cu_6Sn_5 and Cu_3Sn , which precipitate at different stages of the reaction in Sn-Cu alloys. Cu_3Sn needs high amounts of Cu and higher temperature than Cu_6Sn_5 (Ref 44). Cu_3Sn is usually formed from the growth of Cu_6Sn_5 (Ref 45). However, the types and amount of intermetallics which form during solidification are determined by

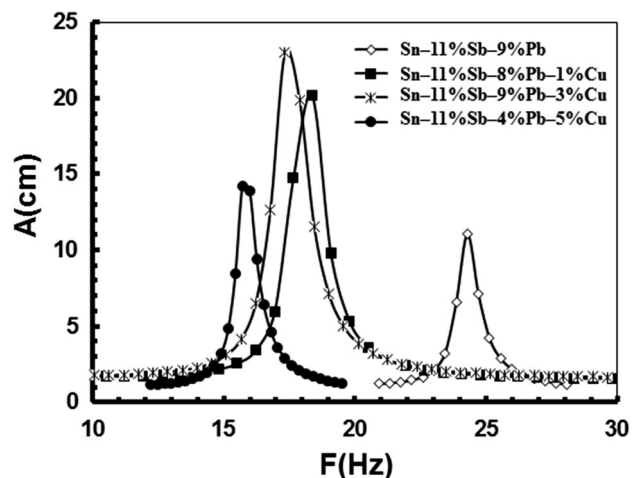


Fig. 5 The resonance curves (the amplitude, A, vs. frequency, F) for melt-spun alloys Sn-11% Sb-(9 - X)%Pb-X%Cu and X = 0,1,3, and 5% Cu

the starting composition and how much copper and other metals have dissolved into the molten of the alloy. Due to the rapid quenching and the different alloying elements in the matrix, this small amount of Cu is increased in our study.

The dissipation of mechanical energy inside the material is called internal friction and it is different from “friction,” which is the resistance against the motion of two solid surfaces relative to each other. To study structural defects and their mobility, transport phenomena, and phase transformations in solids, internal friction is widely used in solid state and physical metallurgy (Ref 46). The results of internal friction, as listed in Table 1, varied slightly. The change in the alloying elements in the materials is the cause of this variation in internal friction. There is an overall increase in the internal friction with increasing the Cu content at the expense of Pb. This can be attributed to the particle refinement that results from the existence of intermetallic compounds (Ref 32).

4. Conclusions

In this paper, the indentation creep and the mechanical properties of Sn-11%Sb-(9 - X)Pb-X%Cu alloys, where X = 0, 1, 3, and 5 wt.%, have been investigated. The change in the microstructure of the β -Sn matrix because of the formation of the SbSn and Cu_6Sn_5 intermetallic compounds affects all measured physical properties, such as elastic modulus and internal friction. Finally, the following conclusions are drawn:

1. With the increase in both time and applied load, the indentation length increases.
2. A regime of individual creep curves is observed for the first and second stages. As the fracture of the samples does not occur, it is not possible to measure the third stage of the curve as generally happens in an ordinary creep test.
3. The indentation creep process can be characterized by the stress exponents. The stress exponents that are obtained from indentation curves range between 2.82 and 5.16.
4. The stress exponent increases with the increase in the concentration of copper at the expenses of lead, which indicates that room-temperature creep takes place less rapidly.
5. The mechanical properties were improved with the increase in the concentration of copper at the expenses of lead.
6. Improvement in the mechanical properties of the alloys that were investigated is primarily due to the formation of the intermetallic compounds SbSn and Cu_6Sn_5 that have smaller particle size than the β -Sn matrix.

References

1. R. Mahmudi and A. Rezaee-Bazzaz, Superplastic Indentation Creep of Sn-Pb-Sb Peritectic, *Mater. Lett.*, 2005, **59**, p 1705–1708
2. X. Li and B.B. Bhushan, A Review of Nanoindentation Continuous Stiffness Measurement Technique and Its Applications, *Mater. Charact.*, 2002, **48**, p 11–36
3. R. Mahmudi, A. Rezaee-Bazzaz, and H.R. Banaie-Fard, Investigation of Stress Exponent in the Room-Temperature Creep of Sn-40Pb-2.5Sb Solder Alloy, *J. Alloy Compd.*, 2007, **429**, p 192–197
4. J.M. Katz and I.S. Buckner, Characterization of Strain Rate Sensitivity in Pharmaceutical Materials Using Indentation Creep Analysis, *Int. J. Pharm.*, 2013, **442**, p 13–19

5. C. Bernard, V. Keryvin, J.C. Sangleboeuf, and T. Rouxel, Indentation Creep of Window Glass Around Glass Transition, *Mech. Mater.*, 2010, **42**, p 196–206
6. R. Mahmudi, A.R. Geranmayeh, H. Khanbareh, and N. Jahangiri, Indentation Creep of Lead-Free Sn-9Zn and Sn-8Zn-3Bi Solder Alloys, *Mater. Des.*, 2009, **30**, p 574–580
7. H. Takagi, M. Dao, and M. Fujiwara, Analysis on Pseudo-Steady Indentation Creep, *Acta Mech. Solida Sin.*, 2008, **21**, p 283–288
8. J. Němeček, Creep Effects in Nanoindentation of Hydrated Phases of Cement Pastes, *Mater. Charact.*, 2009, **60**, p 1028–1034
9. B. Zhao, B. Xu, and Z. Yue, Indentation Creep-Fatigue Test on Aluminum Alloy 2A12, *Mater. Sci. Eng. A*, 2010, **527**, p 4519–4522
10. D. Dorner, K. Roller, B. Skrotzki, B. Stockhert, and G. Eggeler, Creep of a TiAl Alloy: A Comparison of Indentation and Tensile Testing, *Mater. Sci. Eng., A*, 2003, **357**, p 346–354
11. J. Wu and Y. Jinhongpi, On Indentation Creep of Two Cu-Based Bulk Metallic Glasses via Nanoindentation, *Phys. B*, 2003, **421**, p 57–62
12. Y.J. Liu, B. Zhao, B.X. Xu, and Z.F. Yue, Experimental and Numerical Study of the Method to Determine the Creep Parameters from the Indentation Creep Testing, *Mater. Sci. Eng. A*, 2007, **456**, p 103–108
13. R. Mahmudi, A.R. Geranmayeh, M. Bakherad, and M. Allami, Indentation Creep Study of Lead-Free Sn-5%Sb Solder Alloy, *Mater. Sci. Eng. A*, 2007, **457**, p 173–179
14. M. Gan and V. Tomar, Role of Length Scale and Temperature in Indentation Induced Creep Behavior of Polymer Derived Si-C-O Ceramics, *Mater. Sci. Eng. A*, 2010, **527**, p 7615–7623
15. C. Herring, Diffusional Viscosity of a Polycrystalline Solid, *J. Appl. Phys.*, 1950, **21**, p 437–445
16. R.L. Coble, A Model for Boundary Diffusion Controlled Creep in Polycrystalline Materials, *J. Appl. Phys.*, 1963, **34**, p 1679–1682
17. H. Zaki, A. Abdel-Daiem, Y. Swilem, F. El-Tantawy, F. Al-Marzouki, A. Al-Ghamdi, S. Al-Heniti, F. Al-Hazmi, and T. Al-Harbi, Indentation Creep Behavior and Microstructure of Cu-Ge Ferrites, *Mater. Sci. Appl.*, 2011, **2**, p 1076–1082
18. J. Weertman, The Creep Strength of the Earth's Mantle, *Rev. Geophys. Space Phys.*, 1970, **8**, p 145–168
19. R. Roumina, B. Raesisinia, and R. Mahmudi, Room Temperature Indentation Creep of Cast Pb-Sb Alloys, *Scripta Mater.*, 2004, **51**, p 497–502
20. A. Zeren, E. Feyzullahoglu, and M. Zeren, A Study on Tribological Behaviour of Tin Based Bearing Material in Dry Sliding, *Mater. Des.*, 2007, **28**, p 318–323
21. M.O. Bora, O. Coban, T. Sinmazcelik, V. Günay, and M. Zeren, Instrumented Indentation and Scratch Testing Evaluation of Tribological Properties of Tin-Based Bearing Materials, *Mater. Des.*, 2010, **31**, p 2707–2715
22. A. Zeren, Embeddability Behaviour of Tin-Based Bearing Material in Dry Sliding, *Mater. Des.*, 2007, **28**, p 2344–3350
23. M. Kamal, A. El-Bediwi, and M.R. El-Shobaki, Influence of Alloying Elements on Structure and Some Physical Properties of Quenched Sn-Sb Alloy, *Radiat. Eff. Defect Solids*, 2006, **16**, p 549–557
24. A. El-Bediwi, A.R. Lashin, M. Mossa, and M. Kamal, Indentation Creep and Mechanical Properties of Quaternary Sn-Sb Based Alloys, *Mater. Sci. Eng. A*, 2011, **528**, p 3568–3572
25. S. Ishihara and K. Tamura, Effect of Amount of Antimony on Sliding Wear Resistance of White Metal, *Tribol. Int.*, 2010, **43**, p 935–958
26. V.I. Tkatch, A.I. Limanovskii, S.N. Denisenko, and S.G. Rassolov, The Effect of the Melt-Spinning Processing Parameters on the Rate of Cooling, *Mater. Sci. Eng. A*, 2002, **323**, p 91–96
27. E. Schreiber, O.L. Anderson, and N. Soga, *Elastic Constant and Their Measurements*, McGraw-Hill, New York, 1973, p 82
28. M. Kamal, H.F. Abosheisha, and T. Medhat, Some Physical Measurements by Using Rough Sets Techniques, *Int. Heat Treat. Surf. Eng.*, 2010, **IX(2)**, p 13–22
29. M. Kamal, A. El-Bediwi, A.R. Lashin, and A.H. El-Zarka, Copper Effects in Mechanical Properties of Rapidly Solidified Sn-Pb-Sb Babbitt Bearing Alloys, *Mater. Sci. Eng. A*, 2011, **530**, p 327–333
30. B.R. Rehani, P.B. Joshi, K.N. Lad, and A. Pratap, Crystallite Size Estimation of Elemental and Composite Silver Nano-Powder Using XRD Principles, *Indian J. Pure Appl. Phys.*, 2006, **44**, p 157–161
31. L.F. Drummy, B.L. Farmer, and R.R. Naik, Correlation of the b-sheet Crystal Size in Silk Fibers with the Protein Amino Acid Sequence, *Soft Matter*, 2007, **3**, p 877–882

32. A.R. Lashin, M. Mossa, A. El-Bediwi, and M. Kamal, Study of Some Physical Properties of the Rapidly Solidified Sn–Sb–Cu–Zn Alloys, *Mater. Des.*, 2013, **43**, p 322–326
33. W.D. Callister, *Fundamentals of Materials Science and Engineering an Interactive*, Wiley, New York, 2001, p 207
34. I. Lichioiu, B. Peter, and M. Varga, Rosso, Preparation and Structural Characterization of Rapidly Solidified Al–Cu Alloys, *J. Mater. Sci. Technol.*, 2014, **30**, p 394–400
35. T. El Ashram, The Role of Silver Additions in Formation of Sn–Bi–Ag Semiconductor Alloys by Rapid Solidification, *Mater. Sci. Appl.*, 2015, **6**, p 228–233
36. R.A. Higgins, *Properties of Engineering Materials*, Edward Arnold, London, 1977, p 342
37. R. Mahmudi, M. Pourmajidian, A.R. Geranmayeh, S. Gorgannejad, and S. Hashemizadeh, Indentation Creep of Lead-Free Sn–3.5Ag Solder Alloy: Effects of Cooling Rate and Zn/Sb Addition, *Mater. Sci. Eng. A*, 2013, **565**, p 236–242
38. M.E. Kassner and M. Perez-Prado, *Fundamentals of Creep in Metals and Alloys*, Elsevier, Amsterdam, 2004, p 7
39. A. Juhasz, P. Tasnadi, and I. Kovacs, Superplastic Indentation Creep of Lead-Tin Eutectic, *J. Mater. Sci. Lett.*, 1986, **5**, p 35–36
40. M. Nakamura and K. Kimura, Elastic Constants of TiAl₃ and ZrAl₃ Single Crystals, *J. Mater. Sci.*, 1991, **26**, p 2208–2214
41. Y.L. Zhou, M. Niinomi, and T. Akahori, Effects of Ta Content on Young's Modulus and Tensile Properties of Binary Ti–Ta Alloys for Biomedical Applications, *Mater. Sci. Eng. A*, 2004, **371**, p 283–290
42. V.C. Srivastava, A. Upadhyaya, and S.N. Ojha, Microstructural Features Induced by Spray Forming of a Ternary Pb–Sn–Sb Alloy, *Bull. Mater. Sci.*, 2000, **23**, p 72–78
43. M. Kamal, A. Abdel-Salam, and J.C. Rieri, Modification in Tin-Antimony Alloy, *J. Mater. Sci.*, 1984, **19**, p 3880–3886
44. W.Y. Chen, T.T. Chou, W. Tu, H.C. Chang, C.J. Lee, and J.G. Duh, Retarding the Cu–Sn and Ag–Sn Intermetallic Compounds, by Applying Cu–xZn Alloy on Micro-bump in Novel 3D-IC Technologies, *Mater. Sci.: Mater. Electron.*, 2015, **26**, p 2357–2362
45. Q. Yin, F. Gao, Z. Gu, E.A. Stach, and G. Zhou, In Situ Visualization of Metallurgical Reactions in Nanoscale Cu/Sn Diffusion Couples, *Nanoscale*, 2015, **7**, p 4984–4994
46. M.S. Blanter, I.S. Golovin, H. Neuhauser, and H.R. Sinning, *Internal Friction in Metallic Materials, A Handbook*, Springer, Berlin, 2007, p 1